Epidemiology and Infection, Chaos theory applied to the outbreak of Covid-19: an ancillary approach to decision-making in pandemic context, *S. Mangiarotti, M. Peyre, Y. Zhang, M. Huc, F. Roger, Y. Kerr.*

Supplementary Material

This PDF file includes:

Supplementary Material 1-Detailed contextualization

Supplementary Material 2-Materials and Methods

Supplementary Material 3-Data correction for country inter-comparison

Supplementary Material 4-Dynamical regime

Supplementary Material 5-Other Models $\mathbf{M_2}$, $\mathbf{M_3}$, $\mathbf{K_1}$, $\mathbf{K_2}$ and $\mathbf{K_3}$

Supplementary Material 6-Case fatality rate

Supplementary Material 7-Canonical models

Supplementary Material 8-Italy Covid-19 models $\mathbf{I_1}$ to $\mathbf{I_5}$

Supplementary Material 9-Comparative analysis

Figs. S1 to S15

Tables S1 to S5

Supplementary Material 1- Detailed Contextualization

As for numerous infectious diseases, several of the variables involved in the dynamic of the Covid-19 epidemic, although possibly obvious, are known to be quite difficult to observe: for diseases such as Covid-19, infectious people may not develop any clear symptoms, and susceptible people may be detected only once infected by the disease. Another compartment difficult to observe but commonly met in epidemic and surely involved in the Covid-19 epidemic is the compartment corresponding to exposed stage which relies to people having been infected but whom are not yet infectious themselves. Population may also be separated in classes depending on their age or social status to account for specific susceptibility due to it, or to model the transfer between different groups. It was found in particular for the Covid-19 disease that elder people were more susceptible to develop severe stages of the disease whereas severe stages were relatively rare among children whom may often be healthy carriers; It was also observed that health-care personal could constitute a specific class of people with higher susceptibility due to their direct exposure to the infectious people. The use of external compartments may also be useful to express the influence of social events that may strongly contribute to the epidemic, such as the travels associated to the New Year in China or sports and religious gatherings in France or Italy. Couplings to wild or domestic species may also play an important role, though, for the present epidemic, this coupling may probably have taken place at the earlier development of the epidemic only, and is no longer in progress. In some contexts, the anthropological dimension may also have an important influence on the epidemic (as it could be observed for other diseases such as Ebola Virus Disease), although few elements could be established clearly yet in this sense for the Covid-19. The situation of the health systems may also play an important role in the monitoring of the epidemic, both individually in its ability to deal with complex and severe

cases, and collectively in its capacity to deal with a more or less large number of cases with various degrees of infection. Last but not least, the epidemic may also importantly depend on the policies and on the calendar of the measures taken at both government and local scales to eradicate the epidemic and on the practical application of these measures.

Once the main variables potentially identified, the question of the governing equations can be another very hard question: how to formulate their dynamical couplings. Numerous model structures have been introduced to consider these quite varied situations. However, these formulations are all based on *a priori* structures. In other words, the processes and their mathematical formulations are assumed to be clearly known which is generally far to be the case, especially when a new disease is concerned. Moreover, once the model formulation has been chosen, a careful parameterization is required. When this parameterization cannot be performed numerically, either due to intrinsic limitations of the observations (inexistent observations of some compartments, poor quality and shortness of the observational dataset, etc.) parameters may have to be borrowed from other contexts or studies (e.g. parameters calibrated on Influenza applied to Covid-19) or chosen based on theoretical considerations (e.g. statistical hypothesis). In such conditions, simulations will be, at best, qualitative. If all the compartments of the model are observed, and data are of sufficiently good quality, a practical calibration may be performed numerically. Unfortunately, it is generally not the case because of the unobserved variables previously mentioned upper in the text. Moreover, under hypothetically ideal situations about the observations, even if all the variables can be observed, an adequate calibration cannot be reached if the governing equations were not chosen adequately. It is therefore necessary to cope with a cross-challenge: to find a model structure and parameterization adapted not only to the proper

dynamical behaviour but also to the observed data set, that is, in few words, adapted to the practical problem.

Various methodologies have been developed to analyse data sets without strong *a priori* knowledge. Artificial Neural Networks, and in particular deep learning, have proven to be very powerful for the modelling in numerous domains. These may provide an alternative approach to the compartment models of pre-fixed structures and to individual based simulations. However, there skills are known to be highly dependent on the training samples and often require an important quantity of data which is rarely available in epidemiology; such data may even be especially scarce as far as a new disease is concerned. Moreover, these approaches generally lead to black bow models, that is, efficient predictive models which functioning cannot be assessed. Their ability can thus be very useful to perform forecasts, but relatively poor to understand the dynamical behaviours at work.

Supplementary Material 2-Materials and Methods

1. Theoretical background

1.1. Chaos theory

The theory of nonlinear dynamical systems – or chaos theory – has its origins in the work of the French mathematician Henri Poincaré who was the first one to understand how a system can be both at the same time deterministic (*i.e.* the current state of a studied system at time t entirely determines its immediate future state at time $t + \delta t$) and unpredictable at long term. Chaos theory is very well adapted to study real world dynamics because particularly well designed theoretically to study deterministic dynamics that are poorly predictable at long term (Statistical approaches may constitute an alternative to study instable dynamics, but unfortunately abandoning the deterministic part underlying the dynamical behaviour). Striking examples of such deterministic but unpredictable behaviours could be reproduced numerically in the sixties by Edouard N. Lorenz [1] and Otto E. Rössler [2,3]. René Lozi [4] proved that chaotic behaviours could be produced up to the ultimate precision limits of computers. Contrarily to mathematical approaches – which aim is most often to obtain the analytic solutions from studied equations – chaos theory fosters the use of the phase space (or state space). This orientated space is particularly important because it enables a geometric representation of all the states of a dynamical system, independently of time which permits a qualitative representation of the dynamics. Usefully, when the original equations of a studied behaviour are unknown, this space can be reconstructed directly from observational time series. Furthermore, under appropriate conditions, even if several of the system original variables are unknown (or just unavailable), this phase space still can be reconstructed from a subset of observational time series, potentially a

single one [5-7]. Finally, to extract a model from observational time series, observational variables should also enable a good observability of the original equations of the underlying dynamic [8,9].

The global modelling technique aims to obtain differential, discrete or delay models from observational time series. It takes its background from statistics and electronic [10,11]. Its differential form was introduced in the early 1990s [12] to obtain models from single time series. Although it has proven early to be applicable to theoretical and experimental time series [13], it is only in the 2000s that it could be applied to observational data from environmental conditions [14,15] and its applications to multiple time series from real environmental conditions is even more recent [16]. The interest to apply this approach can be multiple. It can be used to detect couplings between observational variables [17], to (re-)formulate these couplings algebraically [18] and, potentially, to understand these couplings based on the reconstructed equations, by inference [16].

1.2 The global modelling technique

In practice, applied to multiple time series, the approach consists in retrieving a set of differential equations in the form $\dot{x}_i = f_i(x_1, x_2, .., x_n)$, with $i = 1..n$, where the dot denote the derivatives with respect to time. When variables are missing, for example if only one variable X_1 is available and defined such as $X_1 = h(x_1, \ldots, x_n)$ with h the measurement function, then, under proper observability conditions, the original system can be rewritten in the canonical form $\dot{X}_{n-1} = F(X, X_1, \ldots, X_{n-1})$ with $X_1 = \dot{X}$, $X_2 = \ddot{X}$, $X_3 = \dddot{X}$, etc. The original system based on variables $(x_1, x_2, .., x_n)$ is then reformulated based on the new set of variables $(X_1, X_2, .., X_n)$. If the original system of equations is known, under appropriate conditions of observability [8], the

canonical form can be derived analytically by using the Lie derivatives $L_f h(x_1,\ldots,x_n) = \sum_{k=1}^{n} f_k(x_1,\ldots,x_n)\frac{\partial h(x_1,\ldots,x_n)}{\partial x_k}$, recursively. The transformation from the original variables to the variables of the canonical system are thus given by $X_i = L_f^{i-1} h(x_1,\ldots,x_n)$.

1.3. Methodology

The GPoM algorithm is used to model and analyse the data set presented in Suppl. Mat. 2. The main goal of this algorithm is to obtain equations from observational time series. Therefore, it does not require a strong *a priori* knowledge about the formulation of the equations underlying the dynamics. In practice, to obtain a set of n equations from n observational time series, the following algorithm parameters are required: (1) The maximum polynomial degree $q^{\max}$, (2) the maximum integration time $T^{\max}$ and (3) the maximum total parameters $N_P{}^{\max}$ allowed for the model. For example, considering $n = 3$ observed variables and a quadratic form will lead to 2^m possible formulations for each equation (with $m = 10$), that is 2^{30} potential models.

The algorithm is based on the following stages: The first equations is initially considered with all its parameters: (1) a Gram-Schmidt procedure is used to estimate its parameters, (2) a leave-one out method is used to identify the less useful monomial (the one enabling the lower residual reduction), (3) this monomial is removed and the resulting formulation is kept as a potential equation. (4) Steps (1) to (3) are repeated until all the monomial are removed from the equation. Thanks to this procedure, the 2^m possible equations will be reduced to $(m+1)$ potential formulations. The same stages (1) to (4) will be repeated for each equation, leading to $(m+1)^n$ potential model formulations, that is, 11^3 potential models in the present case. The number of model to be tested was thus reduced drastically.

A detailed description of the algorithm can be found in [18] where it is shown that the GPoM algorithm is quite efficient to retrieve the compact formulations of the original systems: in most of the cases, all the terms of the obtained structure are indeed present in the original full formulation although some terms of secondary importance may be missing; fallacious detections are rare. It is also proven that polynomial approximations can be obtained from systems of nonpolynomial form. Note that obtaining a model from a stochastic signal is found to be quite improbable.

2. Organization

The analysis presented in the present sudy was performed in two steps. In the first step (A) the epidemic was considered at the China scale. The dynamic of the epidemic was modelled using the global modelling technique to investigate the couplings between three observed variables made available by the Chinese authorities. Models of canonical forms were also applied to single time series and to two time series to detect their coupling.

In a second step (B) the analysis focuses on the number of confirmed cases considering the outbreak in seven provinces in China and three other countries (Japan, South Korea and Italy) where the epidemic has been sufficiently long to provide us with dynamical models of canonical form. The obtained models are then used to produce scenarios for fifteen countries where new focuses have broken out. Observational data are used to validate / invalidate the scenarios and to provide diagnostics and prognostics about the current and future evolution of the outbreaks.

Supplementary Material 3-Data correction for country inter-comparison

Two data sets were used to perform the analyses presented in this study: The data from the National Health Commission of the People's Republic of China [19], and the data from the Johns Hudson University [20], both made available from 21 January 2020 to present (12 April 2020).

The first data set was used to study the epidemic at the scale of China. This data set provides the evolution of the epidemic day by day in China. It gathers an ensemble of variables of daily sampling including the cumulative number of confirmed cases C_Σ, the daily number of new cases C_1, the current number of suspected people, the current number of severe cases s and their day to day variability s_1, the cumulative number of deaths D_Σ and daily deaths D_1. Specific information is sometimes also provided about the geographical origin of the data, but this is not systematic. The methodology used by the authorities to estimate these counts is provided with few details, and without much transparency. As a consequence, suspicions have been raised about possible manipulations, as well as questions about the validity of the data provided by the Chinese authorities. Several elements have alimented these hints, in particular, the early attempt to cover up the issue of an emerging coronavirus, the exclusive control of the communication at the state level with inconsistencies at the transition from province to state, and, more recently, the total number of funeral urns made available to the families after the end of the Wuhan lockdown which seems inconsistent with the announced counts, together with the strong control avoiding any verifications and observation. A new methodology was used from 12 February 2020 (included) up to now to count the number of cases. From 12 February 2020 on, persons having developed clinical symptoms of the Covid-19 were included ([19] 13 February 2020), whereas only the cases identified by standard tests based on nucleic acid were counted before. This sudden compensation generated a strong artefact on the daily counts of confirmed cases and

deaths on 12 and 13 of February 2020. To take into account these additional cases, this sudden contribution was redistributed among the earlier counts by using a multiplicative factor of 1.3 for the cumulated cases and 1.1 for the cumulated deaths on the corresponding period.

The data from the Johns Hudson University [20] were used when considering the epidemic at province scale in China, and in other countries. These data were last downloaded on 12 April 2020. Two variables were considered: the daily cumulated number of confirmed cases $C_{\Sigma}(t)$ and deaths $D_{\Sigma}(t)$. A correction of multiplicative factors 1.4 and 1.1 was applied to the Hubei province to account for the counting methodology change already mentioned. Values were missing for numerous European countries (e.g. Italy, Spain, France, United Kingdom, Switzerland, Netherlands, Denmark and Norway) on 13 March 2020 due to a data harmonization at European scale. There were estimated by linear interpolation. The number of cumulated confirmed cases was not updated correctly on 15 March 2020 in France and UK, it was thus replaced similarly. The contribution of nursing homes was not included in the counts, for France. On DoY 95, this contribution was suddenly added, generating a strong artefact. This contribution was redistributed on the time series using a multiplicative coefficient of 1.35.

Obvious differences were observed between the countries when considering the relationship between the number of cumulated cases and the number of cumulated deaths (Fig. S1). This is obvious when considering the difference between China (in gray) and Italy (in red) (S1a). Several processes can have contributed to such a differential behaviour. It can result from differences in the distribution of the population in age, gender, social position, on capacity of the health system in the country, etc. However, since a detailed sampling of the population is generally impossible, specific protocols are generally used to sample the population. Large differences may thus result from the protocols used to sample the population. Since the

application of this protocol may vary in time and geographically, depending on the situation (saturation in capacity of the health services, limiting stocks of tests, conditions delaying the tests, etc.), it may be difficult to use these original protocols to extrapolate the results at a province or country scale. For this reason, linear regressions were used to inter-calibrate the observations.

The Italian and the Iranian data set were calibrated taking the growing period of Chinese data set as arbitrary reference, and assuming that the number of deaths was suitable without correction. This assumption can have limitations since the methodology may differ from one country to another. Important differences can be expected depending on if deaths in nursing home are accounted or not in hospital only. The correction factor for the number of cumulated cases was estimated to be of 2.45±0.05 for Italy and 1.45±0.05 for Iran (see Fig. S1a). Although the Chinese reference appears adapted when considering very large values of cumulated cases and deaths, its ability to provide a proper reference for small cumulated counts, that is, at the earlier development of the outbreak, appears poorer. Indeed, the increase of deaths at the earlier development of the outbreak appears twice quicker in comparison to the increase of infection at the earlier period of the record, revealing a clear deficit of infection detection. Assuming that this relationship should have remained linear and constant, the number of early undetected cases can be estimated around between 1000 and 2000 cases.

For this reason, the other data sets were calibrated taking the Italian data as direct reference and following the same methodology. Curves before and after calibration are shown in Figures S1b and S1c, respectively. Corresponding coefficients are provided in Table S1. Note that these coefficients can evolve during the propagation of the epidemic since the methodology and the sampling can vary in time (including or not the clinic detection).

The calculation of the time derivatives is required to apply the global modelling technique. The daily time series were thus re-sampled at the hourly time step using cubic splines. This process has proven to be a very efficient procedure for the phase space reconstruction and for the global modelling [23]. The computation of the derivatives was then applied using a Savitzky-Golai filter with a ±4 data points (corresponding to ±4 hours). The successive derivatives obtained from the original time series $C_\Sigma(t)$, $s(t)$ and $D_\Sigma(t)$, will be noted $C_k(t)$, $s_k(t)$ and $D_k(t)$, respectively, with k the derivation degree.

Supplementary Material 4-Dynamical regime

Applying a small parameterization change to model $\mathbf{M_1}$ (Eq. 3 in main text), a phase non-coherent regime is reached, that is, a behaviour in which several pseudo-frequency are involved. This regime is characterized by much more unpredictable behaviour as it can be observed in Figure S2. After the 15-day transient, the three trajectories diverge much quicker than what was observed in Figure 2 (main text).

Supplementary Material 5-Other models

Several models were obtained from variables (C_1, s_1, D_1), all from the same initial conditions (184.363678, 29.799754, 7.768638). The model $\mathbf{M_2}$

$$\begin{cases} \dot{C}_1 = 65.99074685 D_1 - 1.6966388176 D_1^2 + 0.1480196637 s_1 D_1 \\ \qquad - 0.87627987149 C_1 + 0.022842341029 C_1 D_1 - 0.00173419620344 C_1 s_1 \\ \dot{s}_1 = 0.0550673535177817 s_1 D_1 - 0.000823714992557042\ C_1 s_1 \\ \dot{D}_1 = 0.313027803869 D_1 - 0.000105713079 C_1 D_1 - 1.007988313 \cdot 10^{-5} C_1 s_1 + 1.73329184 \cdot 10^{-6} C_1^2 \end{cases} \quad \text{(S1)}$$

has 12 terms, its simulations are shown Fig. S3. The model $\mathbf{M_3}$

$$\begin{cases} \dot{C}_1 = 66.81498537263 D_1 - 1.7245603228 D_1^2 + 0.14721594417 s_1 D_1 \\ \qquad - 0.89162388379 C_1 + 0.02337058406 C_1 D_1 - 0.0017255015863 C_1 s_1 \\ \dot{s}_1 = 0.848314831089 D_1^2 - 0.020249140712 C_1 D_1 + 0.000107801280499 C_1^2 \\ \dot{D}_1 = 0.245260074339929\ D_1 - 6.737844996408 \cdot 10^{-7}\ C_1^2 \end{cases} \quad \text{(S2)}$$

has 11 terms, its simulations are shown Fig. S4. The model $\mathbf{M_4}$

$$\begin{cases} \dot{C}_1 = 66.8149853726 D_1 - 1.7245603228 D_1^2 + 0.147215944170478\ s_1 D_1 \\ \qquad - 0.89162388379 C_1 + 0.02337058406 C_1 D_1 - 0.0017255015863 C_1 s_1 \\ \dot{s}_1 = 0.848314831089027 D_1^2 - 0.0202491407118585 C_1 D_1 + 0.000107801280498737 C_1^2 \\ \dot{D}_1 = 0.253278963164185\ D_1 - 1.13801221078805 \cdot 10^{-5} C_1 D_1 - 5.28439736099 \cdot 10^{-7} C_1^2 \end{cases} \quad \text{(S3)}$$

has 12 terms, its simulations are shown Fig. S5. The model $\mathbf{M_5}$

$$\begin{cases} \dot{C}_1 = 66.8149853726 D_1 - 1.7245603228 D_1^2 + 0.147215944170478\ s_1 D_1 \\ \qquad - 0.89162388379 C_1 + 0.02337058406 C_1 D_1 - 0.0017255015863 C_1 s_1 \\ \dot{s}_1 = 1.4369359975 D_1^2 - 0.0878599667371 C_1 - 0.03750824967 C_1 D_1 + 0.0002549198741 C_1^2 \\ \dot{D}_1 = 0.245260074339929\ D_1 - 6.737844996408 \cdot 10^{-7}\ C_1^2 \end{cases} \quad \text{(S4)}$$

has 12 terms, its simulations are shown Fig. S6.

Several models of canonical form (see Eq. 2 in main text) could also be obtained. The polynomial

$$\begin{aligned} P_{K1}(C_\Sigma,\ C_1,\ C_2) = {} & 1582.18093492246 + 0.000504811960954 C_2^2 - 5.5580461082253\ C1 \\ & - 3.25211135911779 \cdot 10^{-5} C_1 C_2 + 0.000596039491764987 C_1^2 \\ & + 1.20630223143968 C_\Sigma - 0.000103754622181566 C_\Sigma C_1 - 1.24308437097981 \cdot 10^{-5} C_\Sigma^2 \end{aligned} \tag{S5}$$

was obtained model $\mathbf{K_1}$ from the time window (21 January to 9 February 2020), its simulations are shown in Figure S7a. The polynomial

$$\begin{aligned} P_{K2}(D_\Sigma, D_1, D_2) = {} & -2.82771605780217\ D_1 + 0.920196287261328\ D_\Sigma \\ & - 3.09903591887366 \cdot 10^{-5} D_\Sigma D_1 - 1.20725000410706 \cdot 10^{-5} D_\Sigma^2 \end{aligned} \tag{S6}$$

was obtained for model $\mathbf{K_2}$ from the time window (21 January to 12 February 2020), its simulations are shown in Figure S7b. Finally, a canonical model of generalized form was used to investigate the coupling

$$\begin{cases} \dot{C}_\Sigma = C_1 \\ \dot{C}_1 = C_2 \\ \dot{C}_2 = P(C_\Sigma,\ C_1,\ C_2,\ D_\Sigma,\ D_1,\ D_2) \\ \dot{D}_\Sigma = D_1 \\ \dot{D}_1 = D_2 \\ \dot{D}_2 = P(C_\Sigma,\ C_1,\ C_2,\ D_\Sigma,\ D_1,\ D_2) \end{cases} \tag{S7}$$

between these six variables (C_Σ, C_1, C_2, D_Σ, D_1, D_2) and for which the model $\mathbf{K_3}$

$$
\begin{cases}
\dot{C}_\Sigma = C_1 \\
\dot{C}_1 = C_2 \\
\dot{C}_2 = -1.7241077138837 C_1 - 0.0152581047600808\, C_1 D_1 \\
\qquad +0.657403563730002 C_\Sigma - 8.16914452980463 \cdot 10^{-6} C_\Sigma^2 \\
\dot{D}_\Sigma = D_1 \\
\dot{D}_1 = D_2 \\
\dot{D}_2 = -0.0406283337725 D_1^2 + 0.861381073059 D_\Sigma - 0.0053919793449 D_\Sigma D_1 \\
\qquad -8.41844964049054 \cdot 10^{-5} D_\Sigma^2 - 0.00116552183871 C_1 D_1 + 6.76144275852615 \cdot 10^{-6} C_1^2 \\
\qquad -0.00646694141 9 C_\Sigma + 0.000244668243163 C_\Sigma D_1 - 1.12442449021923 \cdot 10^{-6} C_\Sigma D_\Sigma \\
\qquad +\ 6.16211864026507 \cdot 10^{-7} C_\Sigma C_1 - 1.7054628102074 \cdot 10^{-7} C_\Sigma^2
\end{cases}
\tag{S8}
$$

was obtained from the same time window (21 January to 12 February 2020). Its simulations are shown in Figure S7a-b. Interestingly, this model detects a unidirectional coupling between cases and deaths, the former one having a causal action onto the latter, without retroaction, as it can be expected as a first approximation.

Supplementary Material 6-Case Fatality Rate

Model $\mathbf{M_1}$ (see Eq. 3 in the main text) was used to estimate the Case Fatality Rate (CFR) of Covid-19. This model was integrated numerically from 21 February 2020 (DoY 52) to 6 September 2020 (DoY 250). The cumulated number of cases $C_\Sigma(t)$ and deaths $D_\Sigma(t)$ were directly deduced from the daily estimates $C_1(t)$ and $D_1(t)$ (see Fig. S3). The case fatality rate was then directly deduced considering a 5 day delay between the two variables. The analysis shows that the CFR converges to 1.30-1.35 depending on the integration length (from 100 to 230 days). Changing the dynamical regime was found to be marginal. This value is high in comparison to previous estimates ([24] 5 March 2020), but more than twice smaller that the estimates directly deduced from the Chinese data sets from Wuhan suburb to China scale 3.97-4.94 (see Table S2). For this reason, other estimates were tried. Estimates based on models $\mathbf{M_2}$ to $\mathbf{M_5}$ gave very results very similar to model $\mathbf{M_1}$ (1.3% < CFR < 1.5%). Estimates based on a combination of models $\mathbf{K_1}$ and $\mathbf{K_2}$ (CFR ~3.28) or based on model $\mathbf{K_3}$ were found much more convincing (CFR ~5.0%).

Supplementary Material 7-Canonical models

A structure of canonical form (see Eq. (2) in the main text) was used to retrieve a multidimensional model from single time series. The methodology is provided in Suppl. Mat. 2. The polynomials of the models used to perform scenarios are presented hereafter. The following model functions were obtained, for the Hubei province

$$P_{\text{Hubei}}(C_\Sigma, C_1, C_2) = 728.374334674 + 0.12025655855\, C_2 - 2.44374861116086 C_1 + 6.115900961\, C_1 C_2 + 0.67320557758\, C_\Sigma - 6.7065922695 \cdot 10^{-6} C_\Sigma C_2 - 2.14395055039 \cdot 10^{-5}\, C_\Sigma C_1 - 8.42187611295 \cdot 10^{-6} C_\Sigma^2, \quad \text{(Eq. S9)}$$

with initial conditions (617.0938896, 146.4350011, 116.6699932). The projection (C_Σ, C_1) of its phase space is given in Figure S10a; For the Zhejiang:

$$P_{\text{Zhejiang}}(C_\Sigma, C_1, C_2) = 33.02877246 + 0.72175282909\, C_2 - 3.0997963808\, C_1 + 0.01071494081\, C_1^2 + 0.686737990591491\, C_\Sigma - 0.00136034943\, C_\Sigma C_2 - 0.00070734290234 C_\Sigma C_1 - 0.00068054968885 C_\Sigma^2, \quad \text{(Eq. S10)}$$

with initial conditions (26.039364, 14.6265229, –1.089333), see Figure S10b; For the Henan:

$$P_{\text{Henan}}(C_\Sigma, C_1, C_2) = 15.7875118 + 0.037323657 C_2^2 - 2.16550311440939 C_1 - 0.011262814729 C_1 C_2 - 0.00655453369\, C_1^2 + 0.6106396255 C_\Sigma - 0.00068928413 C_\Sigma C_1 - 0.000955568338357319\, C_\Sigma^2, \quad \text{(Eq. S11)}$$

with initial conditions (2.6233721, 0.3184398, 3.27712507), see Figure S10c; For the Jiangxi:

$$P_{\text{Jiangxi}}\left(C_{\Sigma},C_1,C_2\right)=32.204549591+0.49031399622C_2-3.1140961152C_1 \\ +\ 0.002199220326C_1^2+0.68989562079C_{\Sigma}-0.0013919594626C_{\Sigma}C_2 \\ +\ 0.00026427097753C_{\Sigma}C_1-0.00071476276503C_{\Sigma}^2, \quad \text{(Eq. S12)}$$

with initial conditions (9.93751978, 14.1311195, 1.9752268239), see Figure S10d; For the Guangdong:

$$P_{\text{Guangdong}}\left(C_{\Sigma},C_1,C_2\right)=-1.02106445487+0.81072130655C_2-1.395924231C_1 \\ -0.012327743251C_1C_2+0.543560087856C_{\Sigma}-0.0016197665499C_{\Sigma}C_2 \\ -0.0020056527991C_{\Sigma}C_1-0.00090789371754C_{\Sigma}^2, \quad \text{(Eq. S13)}$$

which projection (C_{Σ}, C_1) of the phase portraits is given in Figure S10e with initial conditions (15.36734533, 8.0091208674, 5.6142410724); For the Anhui:

$$F_{\text{Anhui}}\left(C_{\Sigma},C_1,C_2\right)=31.38290829+0.38390685661C_2-3.5311710824C_1 \\ -0.00731724814919C_1^2+0.774413823641C_{\Sigma}-0.0012193215228C_{\Sigma}C_2 \\ +0.001313318079C_{\Sigma}C_1-0.0010396400224C_{\Sigma}^2, \quad \text{(Eq. S14)}$$

with initial conditions (7.3752626332, 1.9460686395, 1.8400134404), see Figure S10f; For the Heilongjiang:

$$P_{\text{Heilongjia ng}}\left(C_{\Sigma},C_1,C_2\right)=-0.45216004565\ C_2-1.7938406094C_1+0.02704335177C_1C_2 \\ -0.0050750328249C_1^2+0.68013328873C_{\Sigma}-0.0012900540558C_{\Sigma}C_2 \\ -0.0017897661 1992496\ C_{\Sigma}C_1-0.00106038366348117\ C_{\Sigma}^2, \quad \text{(Eq. S15)}$$

with initial conditions (2.9464454755, 1.8801103178, 0.80343957214), see Figure S10g; And for South Korea:

$$P_{\text{South Korea}}(C_\Sigma, C_1, C_2) = -2.3996225057 C_1 + 0.0025273468239 C_1 C_2 - 0.0012812217959 C_1^2 + 1.0858468259 C_\Sigma - 0.00038068284318 C_\Sigma C_2 + 3.1133342825 \cdot 10^{-5} C_\Sigma C_1 - 0.00014594323375 C_\Sigma^2, \quad \text{(Eq. S16)}$$

with initial conditions (1.1440650785, 1.0713288594, 0.53117662272), see Figure S10h.

The comparison between models and observations are shown in Figures S10i-j for cumulative cases C_Σ and in S10k-l for daily new cases C_1. Basic statistics for model validation are presented in Tables S3-S4 for C_Σ and C_1, respectively.

Supplementary Material 8-Italy Covid-19 model

Taking into account the data made available 26 March 2020 from the Johns Hopkins University (*i.e.* time series up to 25 March 2020), four canonical models $\mathbf{I_1}$ to $\mathbf{I_4}$ could be obtained for the first time for Italy ([25] Bulletin no 7). An improved version $\mathbf{I_5}$ of these models was obtained on 2 March 2020. Note that, as for the other models, *no* strong a priori structure was used to constrain this model: it was entirely derived from the observational time series, without strong hypotheses. In other words, it is not just a calibration since the dynamic is not assumed to be known. This is an important element to have in mind since such a general polynomial structure can generate a huge diversity of dynamics, such as: highly dissipative chaotic dynamics (e.g. the Lorenz-1963 [1] and Rössler-76 [2] systems), weakly dissipative dynamics (cereal crops attractor [15]), but also SEIR epidemiological models, quasiperiodic and periodic behaviours, among which, numerous of them can be derived analytically [26]. Moreover, contrarily to most of the modelling approaches commonly used, the chaos based approach here used is also independent to the initial conditions: the equations obtained here are deduced from the observed data set but are not specific to the observed initial conditions.

Four numerically integrable models were obtained. Their general equation structure is given by Equations (2) in the main text, with polynomials

$$P_{I1}(C_\Sigma, C_1, C_2) = 235.8603181 - 2.537890524\, C_1 + 0.00012541693084\, C_1 C_2 + 2.9522662766\times10^{-5} C_1^2 + 0.43547233828 C_\Sigma - 1.31622386264564\times10^{-5}\, C_\Sigma C_2 - 1.8756773102\times10^{-6}\, C_\Sigma^2, \quad \text{(Eq. S17)}$$

$$P_{I2}(C_\Sigma, C_1, C_2) = 235.0925272 - 2.52716646641 C_1 + 0.000124997265 C_1 C_2 + 2.642113130882\times10^{-5} C_1^2 + 0.4340714714434\, C_\Sigma - 1.30693954972\times10^{-5} C_\Sigma C_2 + 5.71464460270556\times10^{-7} C_\Sigma C_1 - 1.89712803975814\times10^{-6} C_\Sigma^2, \quad \text{(Eq. S18)}$$

$$P_{I3}(C_\Sigma, C_1, C_2) = 235.5283216548 + 0.246042417278 C_2 - 2.65770740273 C_1 + 6.810976800339 \times 10^{-5} C_1 C_2 + 5.73485453204 \times 10^{-5} C_1^2 + 0.449841284659 C_\Sigma - 9.78612550304 \times 10^{-6} C_\Sigma C_2 - 4.68948606 \times 10^{-6} C_\Sigma C_1 - 1.7151675833 \times 10^{-6} C_\Sigma^2, \quad \text{(Eq. S19)}$$

$$P_{I4}(C_\Sigma, C_1, C_2) = 233.587980099434 + 0.276670713452435 C_2 - 3.62780529127 \times 10^{-5} C_2^2 - 2.61930039204 C_1 + 8.503453508805 \times 10^{-5} C_1 C_2 + 4.332025293903 \times 10^{-5} C_1^2 + 0.447700529125 C_\Sigma - 1.2076698987 \times 10^{-5} C_\Sigma C_2 - 2.041565606308 \times 10^{-6} C_\Sigma C_1 - 1.843458416305 \times 10^{-6} C_\Sigma^2, \quad \text{(Eq. S20)}$$

$$P_{I5}(C_\Sigma, C_1, C_2) = 157.871260954058 + 0.301864656029729 C_2 - 1.462582670896 C_1 + 3.18420349201 \times 10^{-5} C_1^2 + 0.249835293466 C_\Sigma - 2.2772421943 \times 10^{-6} C_\Sigma C2 - 5.7575974104 \times 10^{-6} C_\Sigma C_1 - 6.59948490778 \times 10^{-7} C_\Sigma^2, \quad \text{(Eq. S21)}$$

respectively for Models **I_1**, to **I_5**. All were obtained from the same set of initial conditions (–0.000077827, –0.00033075, 0.00028593). The simulations obtained from model **I_5** are shown in Figure S14, whereas previous simulations obtained from **I_1** to **I_4** can be found in [23] (Bulletin no 7). These simulations suggest that the maximum of the epidemic in terms of daily new cases has been reached and the ending stages can now be estimated for the Italian outbreak, assuming that the control measures will remain stable. Although new clusters cannot be excluded yet, obtaining such a model clearly shows that the main current focuses of Covid-19 in Italy are now stabilizing. Among the four models, models **I_1** and **I_2** can only marginally reproduce the oscillations observed in the original data set and are thus oversimplifying the dynamic. Models **I_3** and **I_4** appear more reliable but were obtained too early to model the plateau reached by the daily number of new cases in comparison to model **I_5**. Based on model **I_5**, it is estimated that the

cumulative number of cases may reach ~454 thousand cases (~376 thousands before correction). Based on this model, the ending stages can also be estimated. The stage corresponding to a level of ~130 new cases per day is estimated for 5 May 2020. This Italian scenario was also applied to France, leading to a cumulative number of cases of ~504 thousand cases (~376 thousand before correction) with a ten day delay. Note however that the last scenarios suggest that France will not reach the Italian scenario. These numbers should thus be slightly lower and the date corresponding to 130 new cases per day should be slightly earlier (see Table S5).

Supplementary Material 9-Comparative analysis

Various modelling approaches have been developed to formulate scenarios with the aim to provide well-grounded arguments for decision making. In particular, for the present Covid-19 pandemic, an Agent Based model initially developed to support pandemic influenza planning, was used to provide a comparison of suppression versus mitigation strategies under real pandemic situation [27]. Such models can simulate the behaviours at various scales, both in time and space and was applied to the UK and the US. Such type of model can include numerous variables and enable realistic simulations. In practice, such models require the identification of the main active agents, and the formulation – at the agents scale – of the main processes at work in the propagation of the disease. These obvious interests will also have some specific limitations. In particular, the main agents and agent properties described in the model will have to be known sufficiently well to provide a complete description of the situation (up to a certain degree of approximation), and to be valid in their formulation, and properly calibrated. Each of these points may meet important difficulties. Essential agents may not always be known (e.g. for the present pandemic: the original source of the contamination, the case-0 of each outbreak, the main vectors, etc.), rough approximations may have to be used to represent the complexity of the situation (for numeric reasons, linear assumptions may have to be fostered, retroactions may be avoided or defined with an extreme caution), data may be missing to calibrate such complicated models (many variables at work, even if under linear approximation, mostly) and numerous assumptions may be required (e.g. locations where the contacts between the agents can take place, parameterization of the infection distance, incubation period, level of infectiousness depending on the agent status, inter-country propagation growth rate, etc.). Finally, the large number of agents and variables involved in this type of model will also require a high

computation cost, which may lead to delay the reaction, and to make the simulation potentially less understandable, and their interpretation possibly more subjective.

The chaos-based approach used in the present study takes the opposite point of view. Instead of assuming the agents (or rather the variables) and the processes at work to be known, its aim is to extract the governing equations from the observations, without any strong a priori hypotheses. Its advantages and drawbacks may thus completely differ and it may thus potentially offer an independent validation while leading to useful discussion otherwise.

The global modelling technique has never been used under operational conditions: the model for the Bombay plague was obtained one century after the Bombay epidemic took place, and the model for the West Africa outbreak of Ebola Virus Disease, although obtained during the outbreak, was published after the outbreak was over. It is thus the first time that this technique is investigated to test its potential for decision making. To do so, the global modelling approach is not used simply as a modelling approach but to perform inter comparisons between primary clusters in Chinese provinces and various countries in Asia and Europe. As it is presently, it cannot be used to establish specific scenarios but to identify the most relevant scenarios among the situations already experienced in other focuses. In other words, it does not have the same potential as the individual based approaches, but it may potentially bring information that other approaches cannot have.

References:

1. **Lorenz EN**, Deterministic non-periodic flow. *Journal of Atmospheric Science* 1963, 20(2): 130–141

2. **Rössler OE**, An Equation for Continuous Chaos, *Physics Letters* 1976, **57**A(5), 397-398.

3. **Rössler OE**, An equation for hyperchaos, *Physics Letters A* 1979, **71**, 155-157.

4. **Lozi R**, Giga-periodic orbits for weakly coupled tent and logistic discretized maps. In: Siddiqi AH, Duff IS, Christensen O eds. *Proceedings Conference International on Industrial and Applied Mathematics* 2007, Modern mathematical models, methods and algorithms for real world systems, New Delhi, 4–6 Dec. 2004, Anamaya Publisher (New Delhi), 80-14.

5. **Whitney H**, Differentiable manifolds, *Annals of Mathematics*, **37**(3), 645-680, 1936.

6. **Takens F**, *Detecting strange attractors in turbulence. In: Rand D.A. and Young L.-S. (eds.). Dynamical Systems and Turbulence, Lecture Notes in Mathematics* 1981, **898**, *Springer-Verlag*, 366-381.

7. **Sauer T, Yorke JA, Casdagli M**, Embedology, *Journal of statistical Physics* 1991, **65**(3-4), 579-616.

8. **Aguirre LA, Letellier C**, Investigating observability poperties from data in nonlinear dynamics. *Physical Review E* 2011; **83**, 066209.

9. **Letellier C *et al.***, A symbolic network-based nonlinear theory for dynamical systems observability, *Scientific Report* 2018, **8**, 3785, DOI:10.1038/s41598-018-21967-w

10. **Billings SA**, Structure detection and model validity tests in the identification of nonlinear systems, *ACSE Report* 1982, **196**, 22.

11. **Aguirre LA, Billings SA**, Retrieving dynamical invariants from chaotic data using NARMAX models, *International Journal of Bifurcation and Chaos* 1995, **9**(2), 449-474.

12. **Gouesbet G, Letellier C**, Global vector-field reconstruction by using a multivariate polynomial L2 approximation on nets. *Physical Review E* 1994, **49**(6), 4955-4972.

13. **Letellier C *et al.***, Topological Characterization and Global Vector Field Reconstruction from an experimental electrochemical system, *Journal of Physical Chemistry* 1995, **99**, 7016-7027.

14. **Maquet J, Letellier C, Aguirre LA**, Global models from Canadian lynx cycles as a direct evidence for chaos in real ecosystems. *Journal of Mathematical Biology* 2007, **55**(1), 21-39.

15. **Mangiarotti S *et al.***, Polynomial search and global modeling: two algorithms for modeling chaos. *Physical Review E* 2012, **86**(4), 046205.

16. **Mangiarotti S**, Low dimensional chaotic models for the plague epidemic in Bombay (1896–1911), *Chaos, Solitons & Fractals* 2015, **81**, 184-196.

17. **Mangiarotti S, Sendiña-Nadal I, Letellier C**, Using global modelling to unveil hidden couplings in small network motifs, *Chaos* 2018, **28**, 123110.

18. **Mangiarotti & Huc**, Can the original equations of a dynamical system be retrieved from observational time series? *Chaos* 2019, **29**, 023133. doi:10.1063/1.5081448.

19. **National Health Commission of the People's Republic of China** (2020). http://www.nhc.gov.cn/yjb/pzhgli/new_list.shtml (Last assessed on 21 March 2020)

20. **Johns Hudson University** (JHU 2020). https://github.com/CSSEGISandData/COVID-19/tree/master/csse_covid_19_data (last assessed on 21 March 2020)

21. **De Salazar P.M., Niehus R., Taylor A., O'Flaherty Buckee C., Lipsitch M.**, Identifying Locations with Possible Undetected Imported Severe Acute Respiratory Syndrome Coronavirus 2 Cases by Using Importation Predictions, *Emerging Infectious Disaeses*, 2020 Jul, 26(7). https://doi.org/10.3201/eid2607.200250

22. **Flaxman S et al.**, Estimating the number of infections and the impact of nonpharmaceutical interventions on COVID-19 in 11 European countries, *Imperial College COVID-19 Team*, 30 March 2020. https://doi.org/10.25561/77731

23. **Mangiarotti S, Zhang Y, Leblanc M**, Is it possible to erroneously detect low-dimensional determinism and chaos from stochastic signals using the global modelling technique? Electronic Supplementary Material ESM1, Chaos theory applied to the modelling of karst springs: first results from univariate time series, *Hydrogrology Journal* 2019, **27**, 2027-2043. https://doi.org/10.1007/s10040-019-01971-8

24. **World Health Organization**. Coronavirus disease (COVID-2019) situation report—30. https://www.who.int/docs/default-source/coronaviruse/situationreports/20200219-sitrep-30-covid-19.pdf?sfvrsn=3346b04f_2 (accessed 5 March 2020).

25. **Bulletins GPoM-epidemiologic**, https://labo.obs-mip.fr/multitemp/bulletin-gpom-epidemiologic/ (last assessed on 2 April 2020).

26. **Lainscsek C, Letellier C, Schürrer C**, Ansatz library for global modeling with a structure selection, *Physical Review E* 2001, **64**, 016206.

27. **Ferguson et al.** (2020). Impact of non-pharmaceutical interventions (NPIs) to reduce COVID19 mortality and healthcare demand. DOI: https://doi.org/10.25561/77482

5

Fig. S1. Relation between Cumulative cases and cumulated deaths

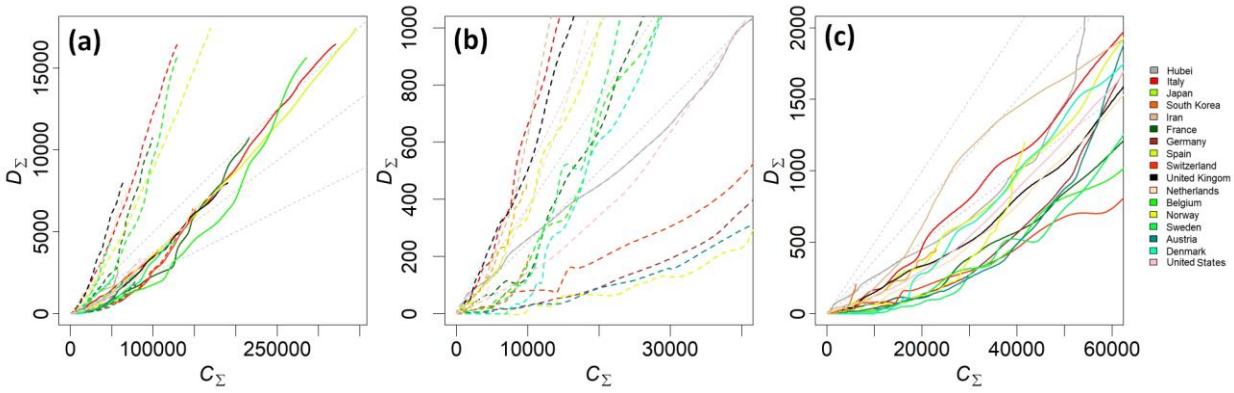

5

Figure S1: Relation between Cumulative cases C_Σ and cumulated deaths D_Σ for Hubei and 16 countries on their full range of values (a) and on selected ranges (b-c). Dashed lines and plain lines refer to uncorrected and corrected cumulated cases, respectively.

5

Fig. S2. Observed and modelled time series under phase non-coherent regime

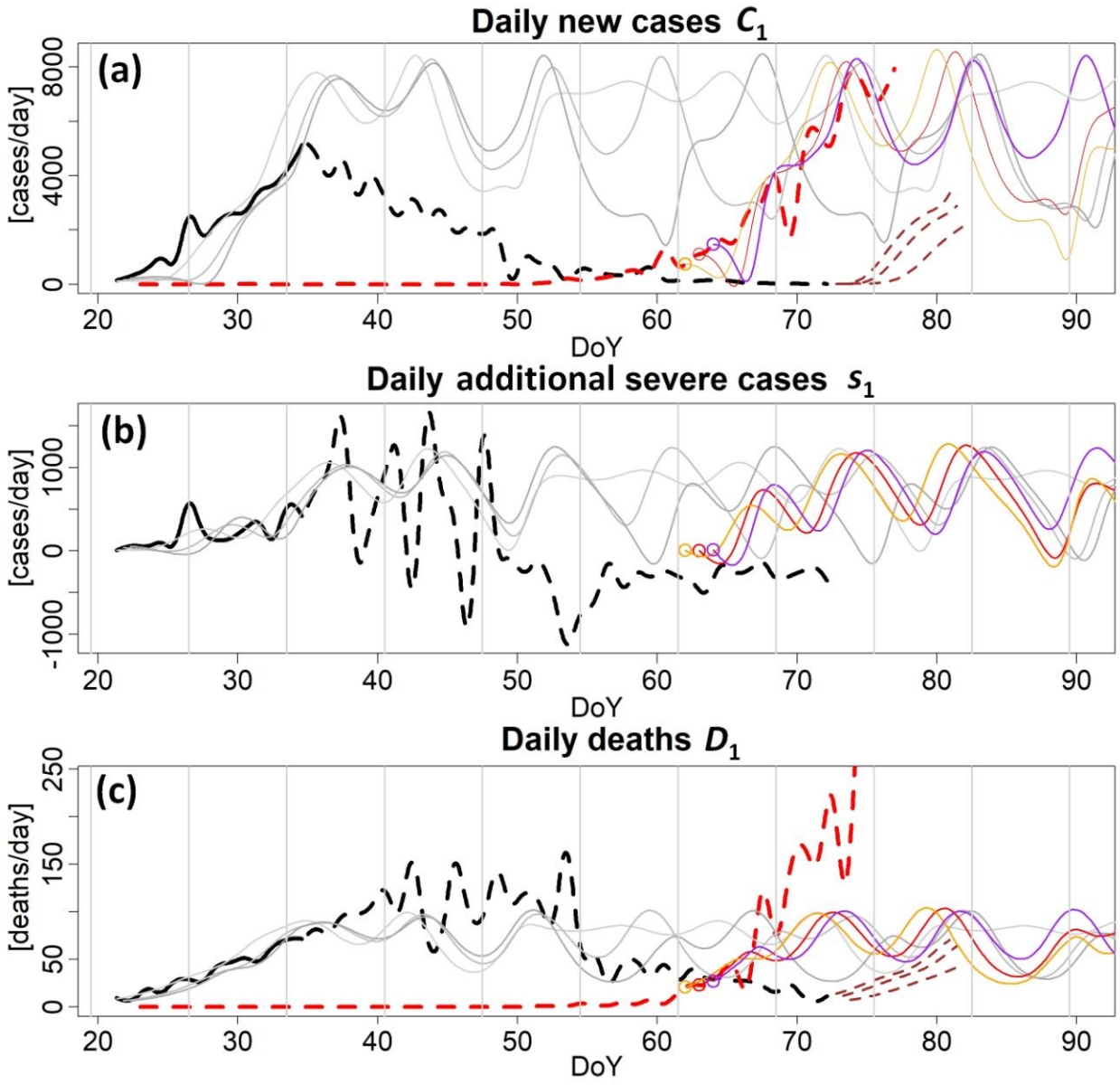

Figure S2: Same as Figure 1 (in the main text) but with a slight parameter change of one monomial, that is +0.154574 s_1D_1 instead of +0.15204 s_1D_1 in Eq. (3). The regime becomes even more chaotic: the topological structure of the updated chaotic attractor involves several foldings instead of a single one before, following the same characteristics as the Rössler-1976 chaotic system[2]. A more detailed topological analysis remains to be performed.

Fig. S3. Model M_2

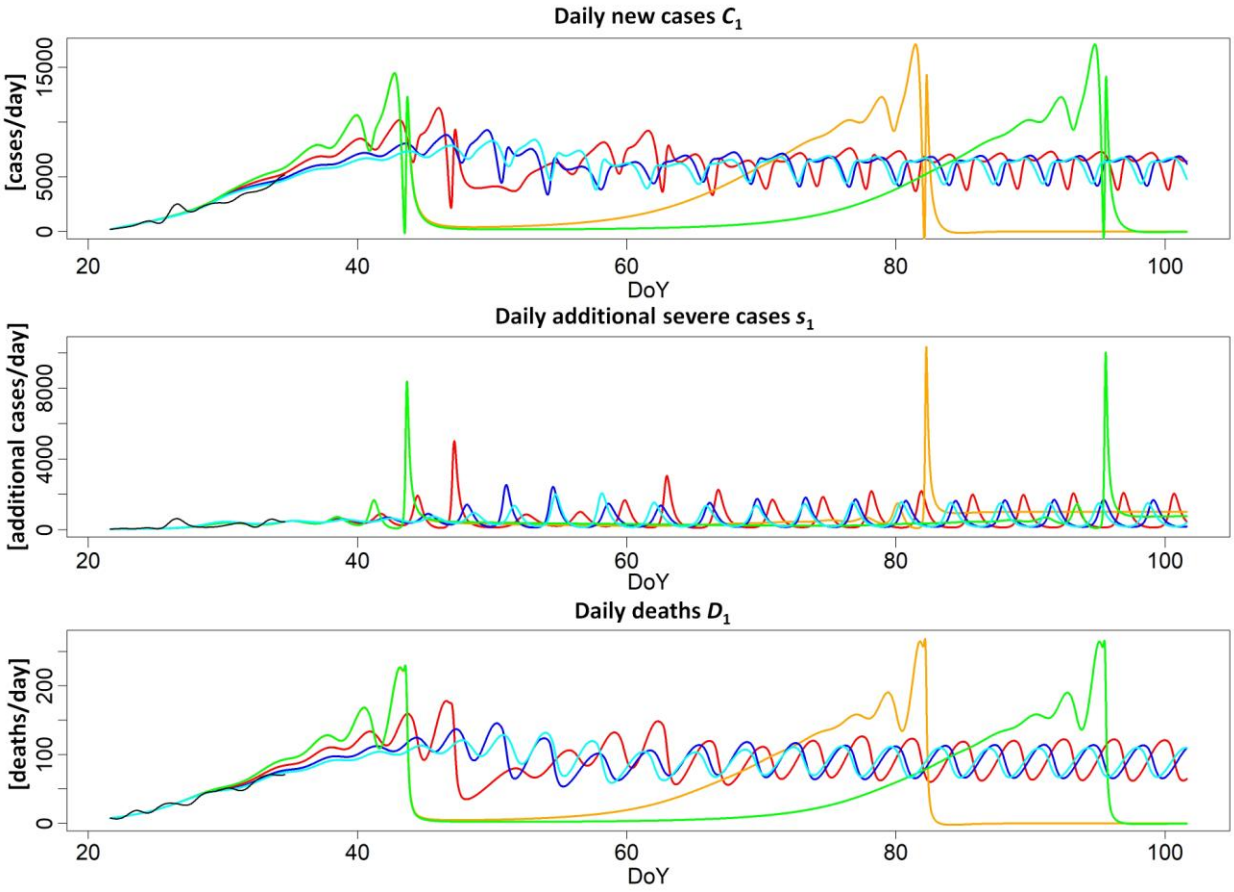

Figure S3: Same as Figure 1 (in the main text) but for model $\mathbf{M_2}$ (see Eq. S1 in Suppl. Mat. 5). The five simulations correspond to slight changes in the parameterization of monomial $\alpha\, D_1^2$ with $\alpha = -1.662197$ (green), $\alpha = -1.662706$ (orange), $\alpha = -1.696639$ (red, unchanged parameter), $\alpha = -1.730572$ (blue), and $\alpha = -1.747538$ (cyan). Interestingly, these modifications can give rise to outbreak decreases with restarts of various delay.

Fig. S4. Model M_3

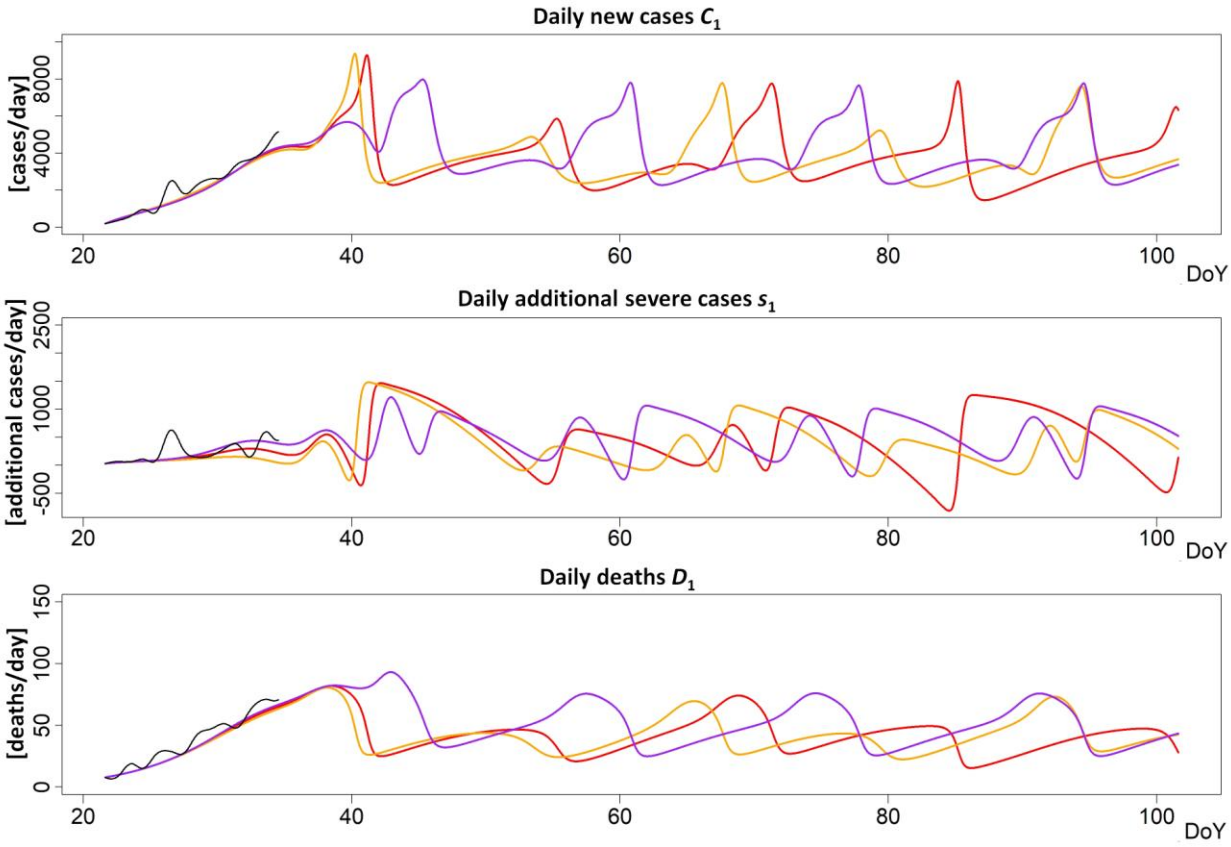

Figure S4: Same as Figure 1 (in the main text) but for model $\mathbf{M_3}$ (see Eq. S2 in Suppl. Mat. 5). The three simulations correspond to slight changes in the parameterization of monomial $\alpha\, D_1^2$ with $\alpha = -1.638332$ (orange), $\alpha = -1.72456$ (red, unchanged parameter) and $\alpha = -1.810788$ (purple).

Fig. S5. Model M_4

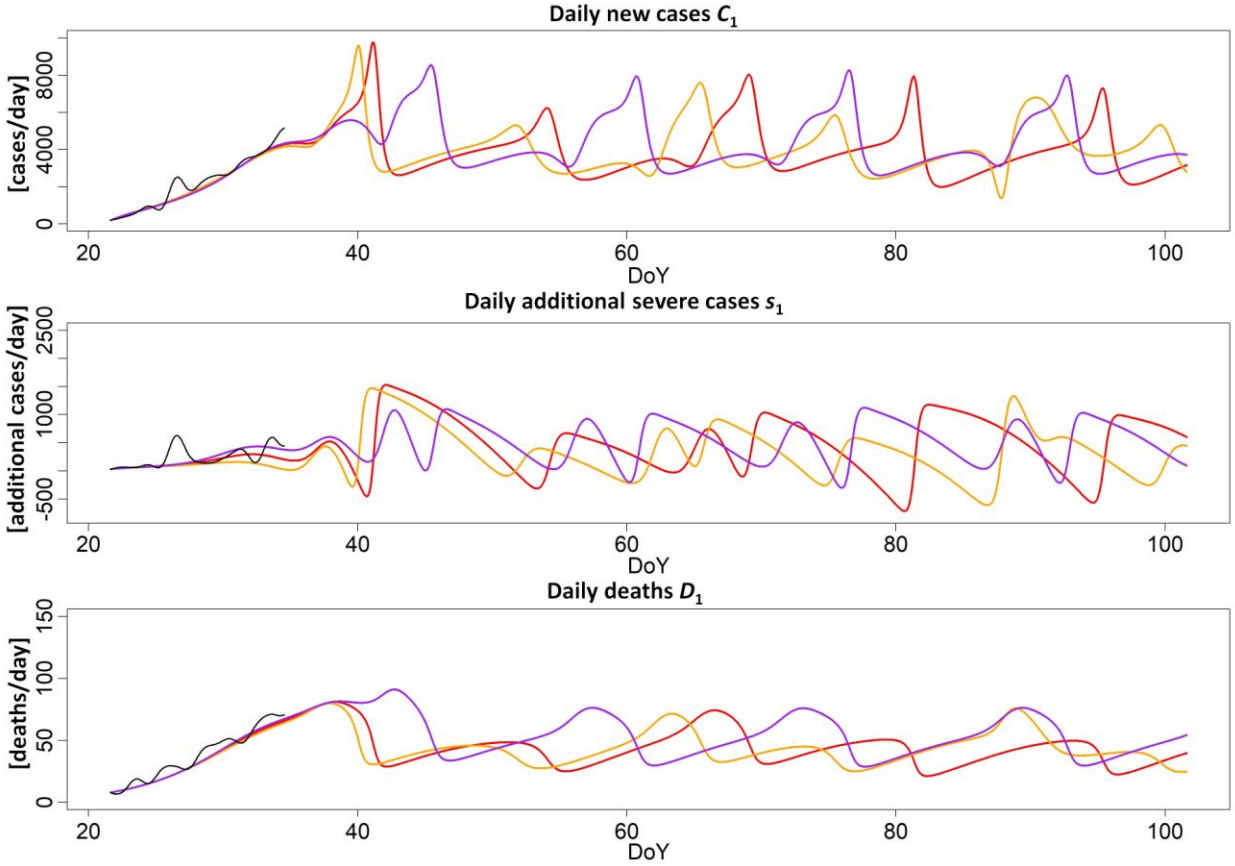

Figure S5: Same as Figure 1 (in the main text) but for model $\mathbf{M_4}$ (see Eq. S3 in Suppl. Mat. 5). The three simulations correspond to slight changes in the parameterization of monomial $\alpha\, D_1^2$ with $\alpha = -1.638332$ (orange), $\alpha = -1.72456$ (red, unchanged parameter) and $\alpha = -1.810788$ (purple).

Fig. S6. Model M_5

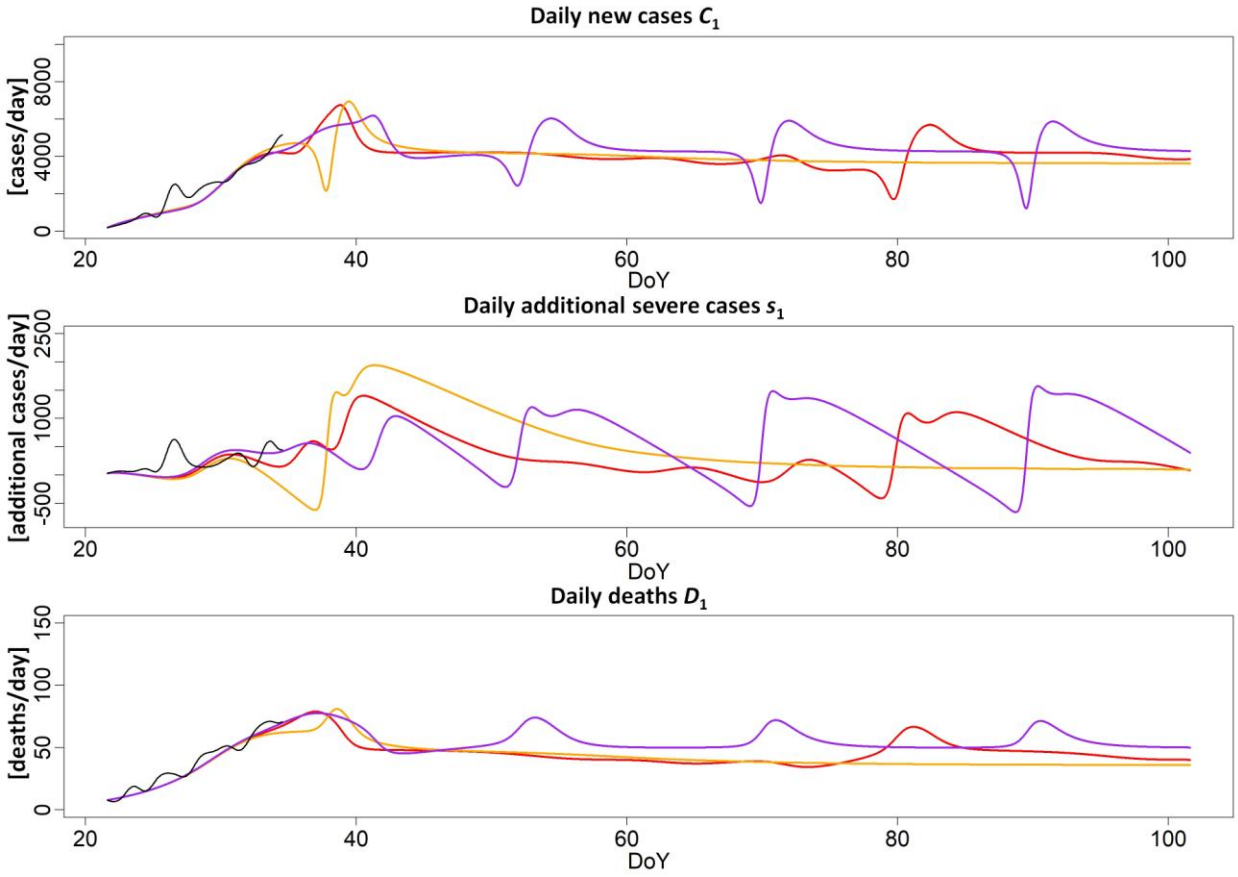

Figure S6: Same as Figure 1 (in the main text) but for model $\mathbf{M_5}$ (see Eq. S4 in Suppl. Mat. 5). The three simulations correspond to slight changes in the parameterization of monomial $\alpha\, D_1^2$ with $\alpha = -1.638332$ (orange), $\alpha = -1.72456$ (red, unchanged parameter) and $\alpha = -1.810788$ (purple).

Fig. S7. Canonical models K_1 for (C_Σ, C_1, C_2), K_2 for (D_Σ, D_1, D_2) and K_3 for the coupling between (C_Σ, C_1, C_2, D_Σ, D_1, D_2).

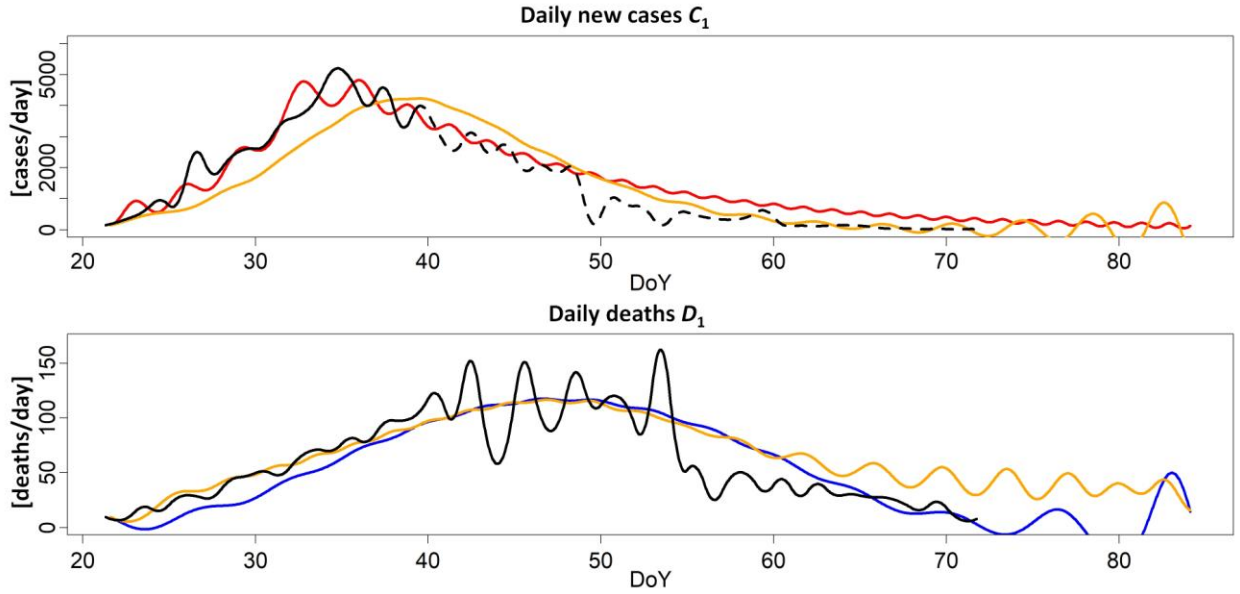

Figure S7: Observed and simulated time series of variables $C_1(t)$ (upper panel) and $D_1(t)$ (bottom panel) with canonical models $\mathbf{K_1}$ (red), $\mathbf{K_2}$ (blue) and $\mathbf{K_3}$ (orange). Corresponding equations are provided in Eqs. S5-S8. One part of the observations corresponds to the identification window (plain lines), and the other part to the validation window (dashed lines).

Fig. S8. Phase portrait and Case Fatility Rate convergence

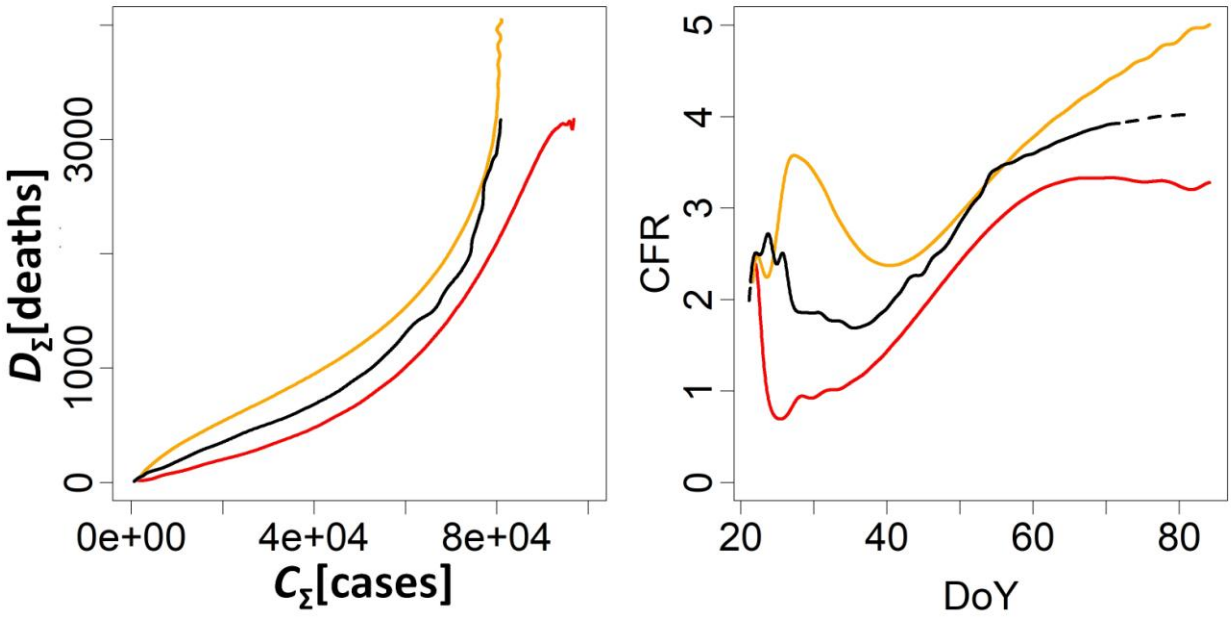

Figure S8: Observed and modelled phase portrait – projection (C_Σ, D_Σ) – (left panel) and Case Fatility Rate convergence (left panel). Estimates based on the combination of models $\mathbf{K_1}$ and $\mathbf{K_2}$ (red) and based on $\mathbf{K_3}$ (orange).

Fig. S9. Case Fatality Rate

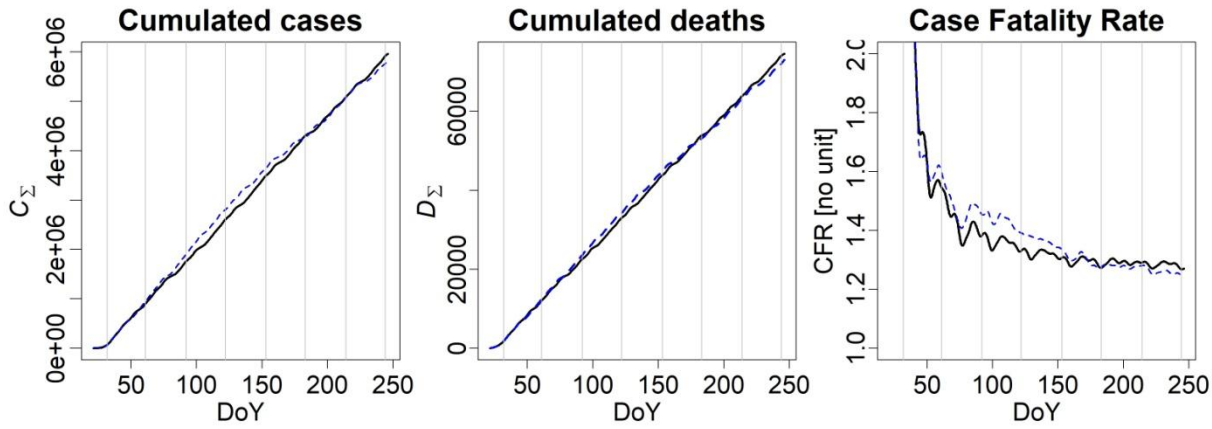

5

Figure S9: Cumulated cases (left panel), cumulated deaths (middle panel) and Case Fatality Rate (right panel) deduced from model **M** (Eq. 1 in the main text). Two simulations are provided, one based on a phase-coherent chaotic regime (black), another one based on a phase-non coherent chaotic regime (blue).

5

Fig. S10. Canonical models validation

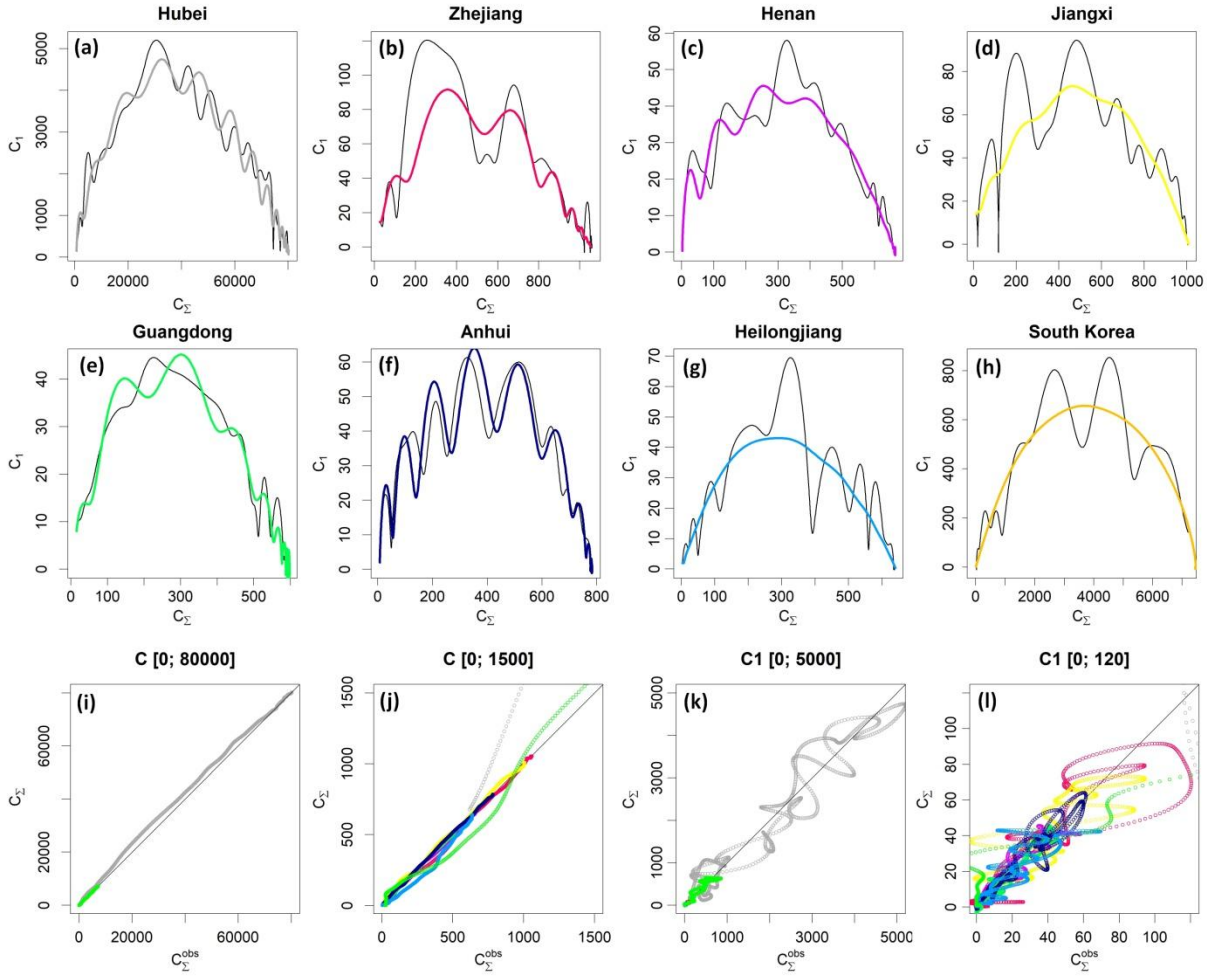

5

Figure S10: Canonical models validation. Original (in colour) and modeled (in black) phase portraits in (C_Σ, C_1) projection for Hubei (a), Zhejiang (b), Henan (c), Jiangxi (d), Gouangdong (e), Anhui (f) and South Korea (h). Scatter plots – modelled $\hat{C}_\Sigma$ versus observed C_Σ^{obs} in (i-j) and modelled $\hat{C}_1$ versus observed C_1^{obs} in (k-l). For more details, see Suppl. Mat. 5.

Fig. S11. Empirical scenarios simulations (variable C_1)

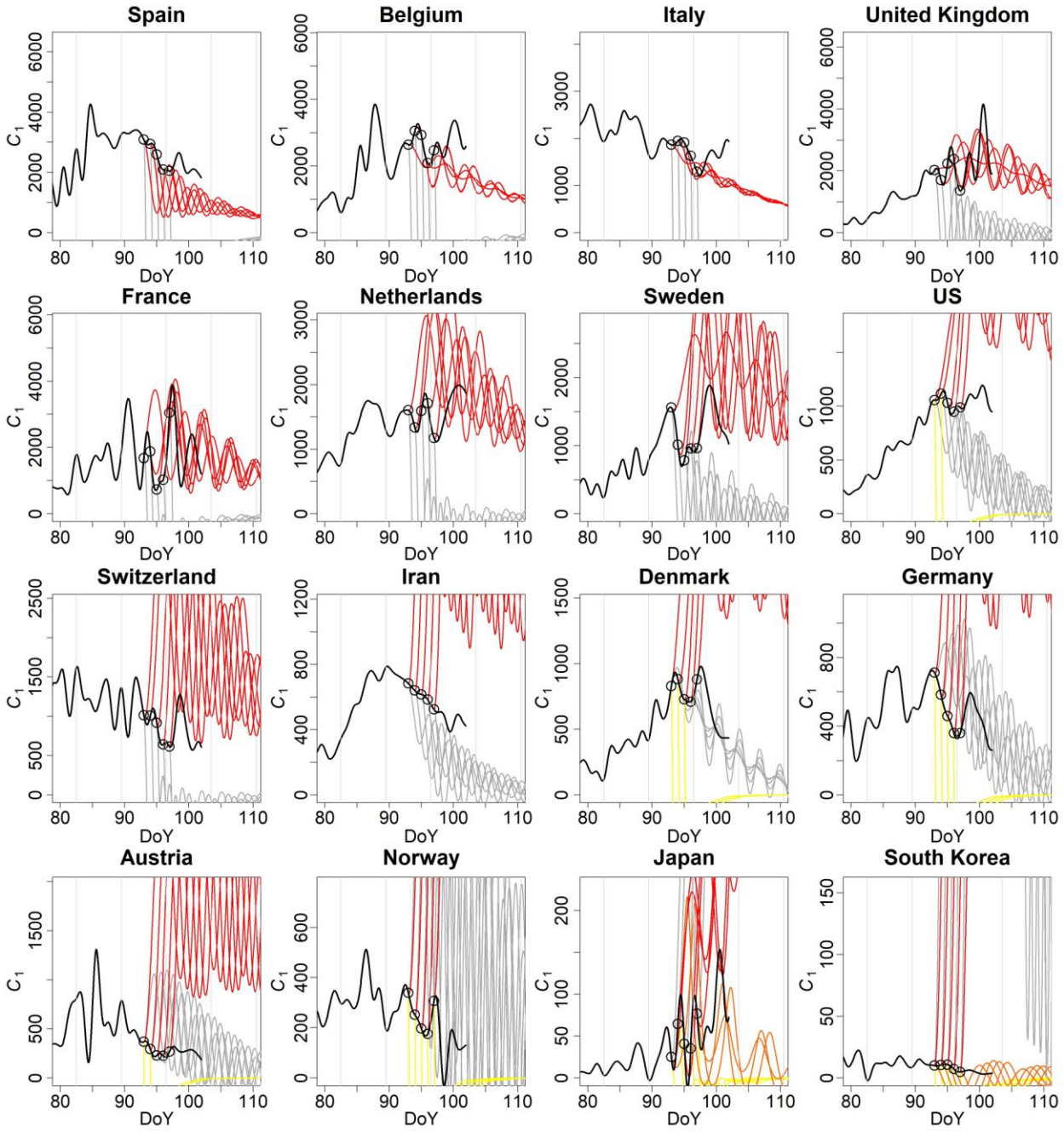

Figure S11: Epidemic curves $C_1(t)$ (daily number of cases) resulting from the scenarios for fifteen countries based on the models obtained from seven Chinese provinces, South Korea, Japan and Italy. For each model, an ensemble of five simulations was run starting from the observational initial conditions (black circle) 2 April (DoY 93) to 6 April (DoY 97) 2020. Observations are in black plain lines. Correction factors used to make the country inter comparison are provided in Suppl. Mat. 2. The Chinese data set is used as reference. Four main scenarios have been kept: the Jiangxi (in yellow), the South Koreas (in orange), the Hubei (in gray) and the Italian scenarios. The other scenarios have been directly rejected.

Empirical scenarios (in color) of the daily number of cases per 10 million population, applied to fifteen countries based on the models obtained for seven Chinese provinces, South Korea, Japan and Italy. Observations are in black plain lines. For each model, an ensemble of five simulations was run starting from the observational initial conditions (black circle) from 2 April (DoY 93) to 6 April (DoY 97). Population size is taken into account but age, geographical distribution and society organization are not. Correction factors were applied to each country to account for the inter-countries discrepancies between the cases and deaths number (see Suppl. Mat. 2). Four main scenarios have been kept: the Jiangxi (in yellow), the South Koreas (in orange), the Hubei (in gray) and the Italian scenarios. The other scenarios were rejected automatically.

Fig. S12. Epidemiologic levels at which control measures have been applied.

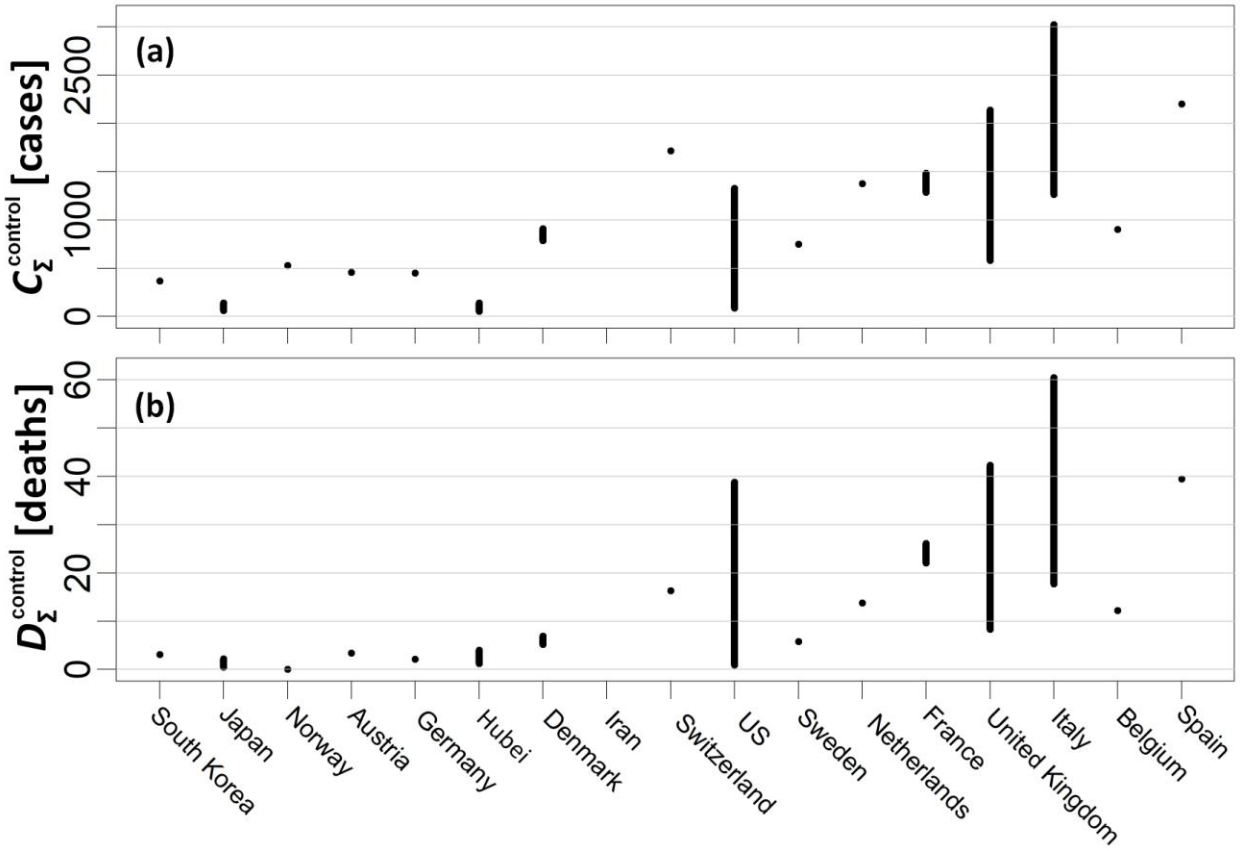

5

Figure S12: Epidemiologic levels at which control measures have been applied, for each country ranked from the smoother to the harder scenario in terms of (a) cumulative number $C_{\Sigma}^{control}$ of cases per million population and (b) cumulative number $D_{\Sigma}^{control}$ of deaths per million population.

Fig. S13. Epidemic curves and control

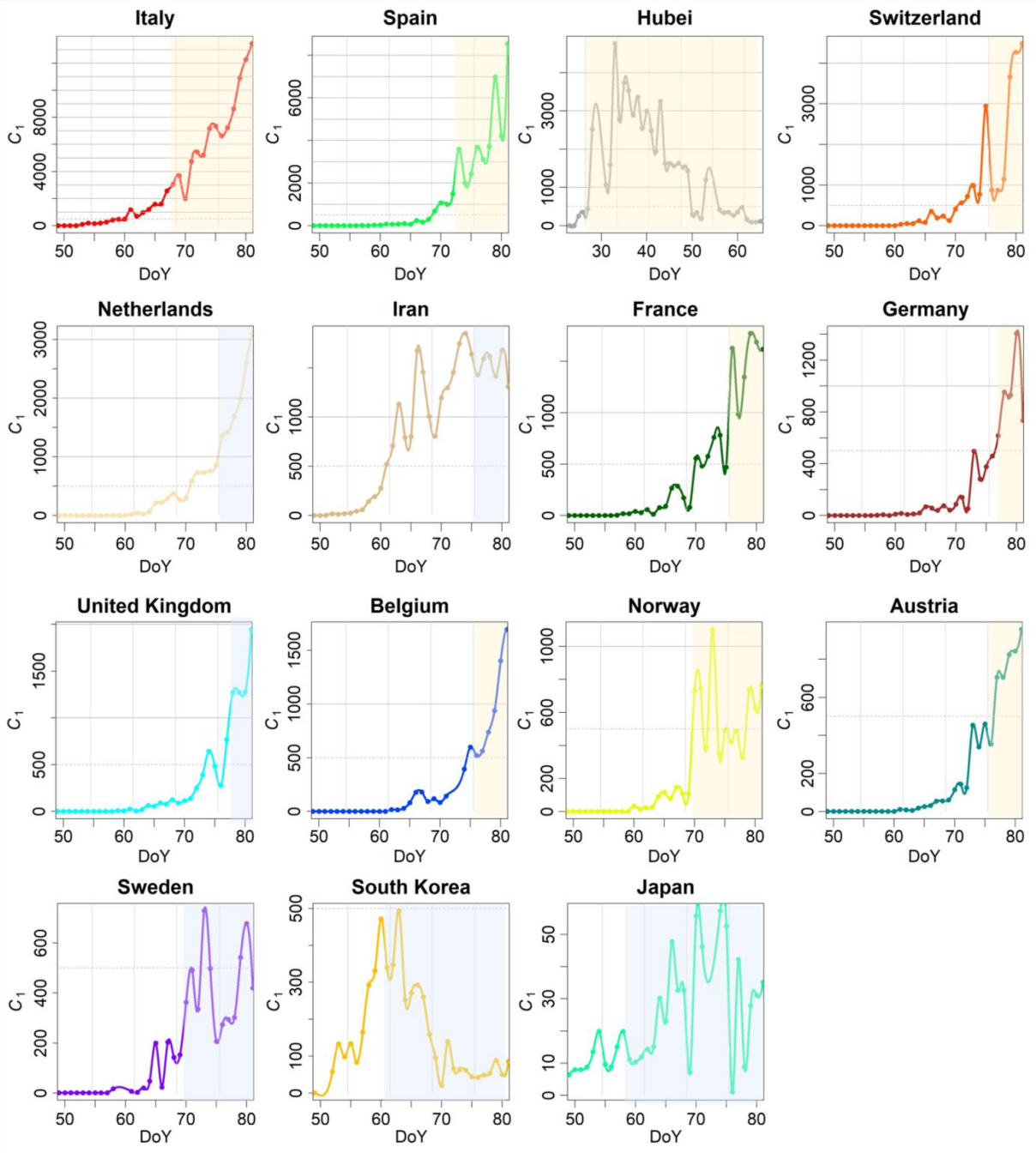

5

Figure S13: Epidemic curves $C_1(t)$ for Hubei province in China and fourteen countries in Asia and Europe. Period with most stringent measures taken by the authorities are shadowed; the level of enforcement of nationwide lockdown varies between countries: from strict state control (yellow) to advice given to citizen and volunteer basis (blue).

Fig. S14. Observed and modelled Covid-19 outbreak in italy

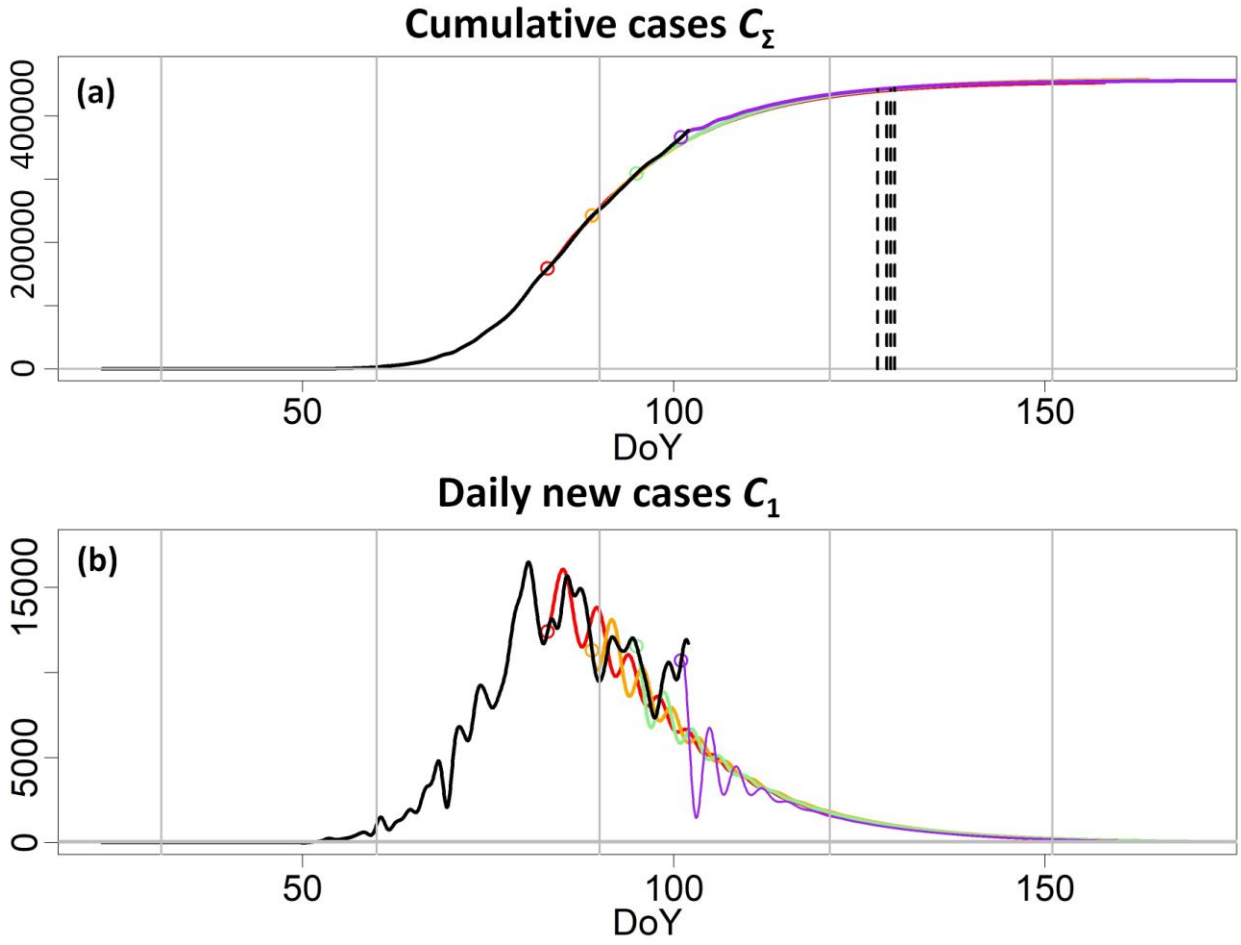

Figure S14: Observed (black line) and Modelled (color lines) cumulative counts of infectious cases $C_{\Sigma}(t)$ (a), and daily new cases $C_1(t)$ (b). The four simulations are from model $\mathbf{M_{I5}}$, initialized from DoY 83 (orange) 89 (red), 95 (green), 101 (purple). Mode details are provided in Suppl. Mat. 6. Dates corresponding to $C_1 = 1000$ are denoted by dashed lines that vary from DoY 127 to 130 (6 to 9 May 2020). More detailed information is provided in Table S5.

Fig. S15. Cumulated cases and deaths per million population ad urban/suburban scales

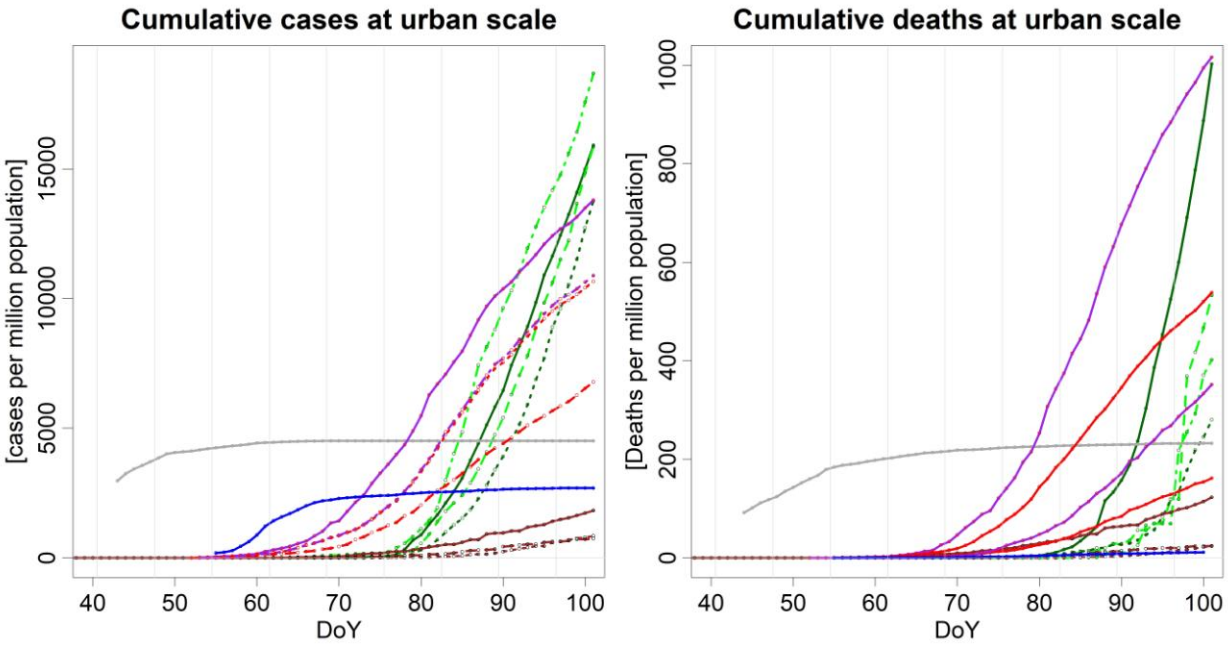

5

Figure S15: Cumulative number of cases per million population (left panel) and cumulated deaths per million population (right panel) (1) at four cities located on the East coast of the United States (in green): New York City (plain line), Nassau (dashed line), Suffolk (dotted line) and Westchester (dashed-dotted line); (2) at three cities on the West coast of the United States (in brown): King (plain line), Santa Clara (dashed line) and Los Angeles (dotted line); (3) at three regions in North Italy (in red/purple): Lombardy (plain line), Veneto (dashed line), Emilia-Romagna (dotted line) and Piedmont (dashed dotted line); (4) at Daegu in South Korea (in blue) and at Wuhan in China (in gray).

Table S1. Correction coefficients

Provinces	Hubei	Zhejiang	Hunan	Henan	Guangdong	Anhui	Jianxi	Heilongjiang
Population (million hab.)	59.17	57.37	68.99	96.05	113.46	63.25	46.48	37.73
Coeff.	1.	1.	1.	1.	1.	1.	1.	1.
Country	United Kingdom	Italy	Iran	Spain	Netherlands	France	Japan	Belgium
Population (million hab.)	66.44	60.48	83.02	49.33	17.42	67.06	125.51	11.52
Coeff.	2.5±0.1	2.48±0.05	2.03±0.05	2.0±0.05	2.6±0.1	2.2±0.05	2.1±0.2	2.2±0.1
Country	Sweden	Switzerland	South Korea	Germany	Denmark	Austria	Norway	United States
Population (million hab.)	10.33	8.57	51.71	80.46	5.82	66.44	5.33	328.24
Coeff.	2.5±0.1	1.0±0.2	0.6±0.1	0.8±0.1	1.4±0.2	0.8±0.2	0.7±0.2	1.1±0.1

Table S1: Population size and correction coefficients (n.u.) applied to the cumulated cases, country by country. The China data set is arbitrarily taken as reference. Note that this will not affect the comparison of the other countries one to another. Coefficients vary from 2.5 in United Kingdom to 0.6 in South Korea. Coefficients greater than one suggest a deficit of detection in comparison to China whereas coefficients lower than one reveal an improved detection. This cannot be simply explained by the population sampling but also by other factors such as the quality of the tests and the time at which tests were performed. Indeed, the detection of the number of infection has proven to be a difficult problem in quantity, quality and in time (e.g.

[21-22]). Assuming that the sampling performed by South Korea is not biased would mean that all the estimates, in the analysis, should be multiplied by 1.7±0.3.

Table S2. Case fatality rate and mortality

	Population (in million)	Total confirmed cases	Total deaths	Case Fatality Rate (in %)	Mortality Rate (in ‰)	Immunity rate (in %)
China	1427.65	81032	3217	3.97	0.00225	0.06-0.6
Hubei	59.17	67798	3099	4.57	0.0524	1.1-11
Wuhan suburb	11.08	50003	2469	4.94	0.2228	4.5-45

Table S2: Case fatality rate, mortality rate and immunity rate resulting from Covid-19 epidemic at China, Hubei and Wuhan suburb scales and estimated on 21 March 2020 (one relatively small part of infected people ~1000 has not recovered yet). Immunity rate was estimated roughly considering a range of 10 to 100 asymptomatic cases for each confirmed case; Even in Wuhan, the herd immunity is not reached.

Table S3. Model validation for cumulative cases

C_Σ	Hubei	Zhejiang	Henan	Jiangxi	Gouangdong	Anhui	Heilongjiang	South Korea
A	0.985	0.997	0.994	0.977	0.989	0.989	1.029	1.007
B	2151.	–1.778	0.6271	22.494	7.6090	10.06	–40.25	–8.272
R^2	0.999	0.997	0.999	0.999	0.999	0.999	0.989	0.999
p-value	< 0.01	< 0.01	< 0.01	< 0.01	< 0.01	< 0.01	< 0.01	< 0.01

Table S3: Statistics for the validation of the canonical models based on the cumulated number of infection C_Σ.

Table S4. Model validation for daily new cases

C_1	Hubei	Zhejiang	Henan	Jiangxi	Gouangdong	Anhui	Heilongjiang	South Korea
A	0.9466	0.801	0.908	0.830	0.978	0.976	0.755	0.906
B	101.3	4.788	1.514	4.104	0.232	0.449	3.807	24.73
R^2	0.923	0.837	0.919	0.844	0.950	0.943	0.721	0.901
p-value	< 0.01	< 0.01	< 0.01	< 0.01	< 0.01	< 0.01	< 0.01	< 0.01

Table S4: Statistics for the validation of the canonical models based on the daily number of new infection C_1.

Table S5. Ending stages

Models	Stage date (in Day of year)				C_{Σ}^{max}	
	C_1 = 130	C_1 = 100	C_1 = 10	C_1 <1	Corrected	Uncorrected
	Italy					
$\mathbf{M}_{I1}$	109	111	121	131	233000	94000
$\mathbf{M}_{I2}$	107	109	118	127	230000	92000
$\mathbf{M}_{I3}$	124	126	144	162	263000	106000
$\mathbf{M}_{I4}$	115	117	131	145	243000	98000
$\mathbf{M}_{I5}$	157	161	193	225	454490	375711
	France					
$\mathbf{M}_{I5}$	168	171	203	236	503934	231162

Table S5: Ending stages (in Day of year) estimated with the four Italian models for various values of daily new cases C_1. Estimated maximum cumulative counts of infectious cases C_{Σ}^{max}; both corrected and uncorrected values (see Table S1) are provided to make the comparison with the official results easier.